












**Absolute frequency measurement of the  $2p^2(^3P)3s^2P-2p^2(^3P)3p^2D^o$  transitions in neutral  $^{14}\text{N}$** 

K. J. Ahrendsen , C. Maruko , K. R. Albert-Aranovich , Q. Berfield-Brewer, A. Esseln , L. Guo, A. E. Ishimwe , Y. Kuzniar, A. E. McKenna , K. J. Soto Villarreal , A. Uprety , L. Vieira da Silva , K. F. Vogt , and W. D. Williams \*

*Physics Department, Smith College, Northampton, Massachusetts 01063, USA*



(Received 14 July 2023; accepted 27 September 2023; published 20 October 2023)

We report absolute frequency measurements on the three excited-state transitions connecting the  $2p^2(^3P)3s^2P_{1/2,3/2}$  and  $2p^2(^3P)3p^2D^o_{3/2,5/2}$  states in neutral  $^{14}\text{N}$  using saturated absorption spectroscopy in a glass cell filled with a mixture of nitrogen and argon gas and driven with a radio-frequency electric field. The absolute transition frequencies are found to be 319 288 834(150), 319 085 445(125), and 316 795 808(140) MHz for the  $1/2-3/2$ ,  $3/2-5/2$ , and  $3/2-3/2$  transitions, respectively. This work represents the saturated absorption measurements for these transitions. These results are approximately a factor of 5 improvement over previous results, despite being conservative estimates. We found that the overlapping hyperfine structure prevented fitting individual spectral features, presenting difficulties for possible future tests of quantum electrodynamics in seven-electron systems. A better understanding of the amplitude behavior of a merged hyperfine structure will allow the extrapolation of the center of gravity frequencies for these transitions to sub-MHz precision using our collected data.

DOI: [10.1103/PhysRevA.108.042815](https://doi.org/10.1103/PhysRevA.108.042815)

**I. INTRODUCTION**

One goal of fundamental atomic physics is to improve the accuracy of our models which describe the universe. A method for accomplishing this task is to use our best models, in this case quantum electrodynamics (QED), to predict the atomic properties of multielectron systems such as absolute energy levels, absolute transition frequencies, and isotope shifts. There are various methods that can be used to solve Schrödinger's equation for a multielectron system, including the variational full-core plus correlation wave-function method (FCPC) [1,2], the variational Monte Carlo method (VMC) [3], the multiconfiguration Hartree-Fock methods (MCHF) [4], the configuration interaction (CI) method [5], and the nonrelativistic quantum electrodynamics (NRQED) method [6]. Arguably the most popular current methods are to use the Hylleraas basis set (Hy) [7–9] and explicitly correlated Gaussians (ECGs) [10,11]. All of these methods can be very precise, but they have key differences which will determine the most accurate method for describing a multielectron system. A more thorough explanation of the different methods can be found in Refs. [5] and [12], and the references therein. Accurate, high-precision experimental results are critical to developing these theoretical methods.

The properties of two-, three-, and four-electron atoms have been calculated using Hylleraas methods; see Ref. [13] as an example of a two-electron system, Refs. [14–17] for examples of three-electron systems, and Ref. [18] for a four-electron system. ECGs have been used to reach both four- [19–24] and five- [25,26] electron systems. Recent work has combined two techniques [27], i.e., a method that accounts for all orders in the binding nuclear strength [28] and NRQED, to improve the accuracy on a wide range of ions

in lithiumlike [29] and heliumlike [30] systems. References [19,20,23,24,26,29,30] included QED corrections.

For four-electron systems, Puchalski *et al.* [31] calculated the absolute energy of the  $2s2p^1P_1^o$  state in beryllium-9 to a precision of  $2.5 \times 10^{-7}$ , which was later confirmed by experiment [32]. The absolute frequency of the  $2s^22p^2P_{1/2}^o - 2s^23s^2S_{1/2}$  transition in boron was recently measured to 2 MHz uncertainty [33,34], confirming theoretical results [26]. For six-electron systems, such as neutral  $^{12}\text{C}$ , many energy levels have been experimentally determined to a precision of  $\sim 10$  MHz or better [35,36].

With theoretical calculations progressing to higher mass elements, high-precision experimental measurements assist these efforts. In the near future, high-precision experimental results in seven- and eight-electron systems, for example neutral nitrogen and oxygen, will be needed to guide the development of theory to accurately describe multielectron systems. These experimental measurements can first be used to guide theory in understanding electron correlation effects, and then later, QED corrections. Based on previous measurements and calculations in other elements, uncertainties on the order of MHz should be sufficiently precise for these purposes; see Refs. [31] and [32] as examples for neutral beryllium-9. In addition, spectroscopy on these light elements across their isotope chain will play a critical role in the development of microscopic nuclear theory [37–40].

Ideally, sub-MHz level precision is desirable for modern high-precision spectroscopy. As presented in this manuscript, additional study and modeling will be needed to reach that precision for seven-electron systems. All isotopes of nitrogen, except for  $^{22}\text{N}$  with a half life of 23 ms, have nuclear spin, with most states having strong coupling to the ground state. To assist these efforts, the hyperfine constants for a number of transitions in  $^{14}\text{N}$  have recently been calculated [41,42]. Singly ionized atomic  $^{16}\text{O}$  has no nuclear spin, but the largest

\*wraven@smith.edu; Legal name: W. D. Raven.

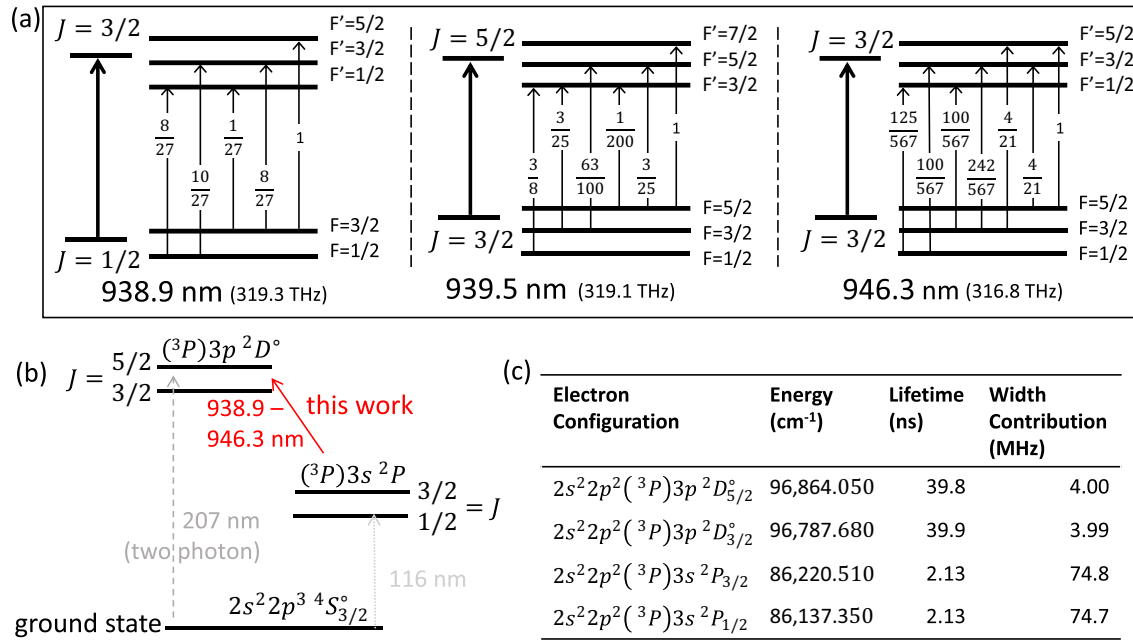


FIG. 1. (a) Simplified Grotrian diagram of the three transitions studied in this manuscript. The fraction inset is the relative intensity of each hyperfine transition. (b) Grotrian diagram showing how transitions can be connected to the ground state. The dotted 116 nm line, which will not be measured, is shown for completeness. (c) Table of details for the four states connected by the three transitions. The lifetimes are calculated from the NIST database [35].

wavelength transition from the ground state is 83.4 nm with a linewidth of  $2\pi \times 137$  MHz [35]. While there has been progress in modeling saturated absorption spectrum [43–45] and quantum interference effects [46] separately, no one has developed a model to accurately simulate a saturated absorption spectrum with a merged hyperfine structure. We believe such a development will be needed to extrapolate the center of gravity to sub-MHz precision in seven-electron systems.

We measure the absolute frequencies of the three transitions connecting the  $2p^2({}^3P)3s \ ^2P - 2p^2({}^3P)3p \ ^2D^\circ$  states; see Fig. 1(a). These transitions can be connected to the ground state by a future two-photon measurement. The studied transitions with respect to the ground state are shown in Fig. 1(b). Figure 1(c) tabulates some of the details of the four states which are involved in these three transitions.

We present a brief history of absolute transition measurements in neutral nitrogen. From the late 1950s through the 1970s, a number of level energies and line classifications were performed on neutral atomic nitrogen [47–51], with further analysis by Eriksson in 1986 [52] and compilation by Moore [53,54]. In 2005, Salumbides *et al.* used a tunable XUV laser near 95 nm [55] to perform Doppler-free spectroscopy on a well-collimated beam of atomic nitrogen to determine the absolute transition frequency from the ground state to 12 excited states with a precision of 150 MHz [56]. In 2020, Lai *et al.* [57] performed VUV Fourier transform spectroscopy using the Dichroïsme Et Spectroscopie par Interaction avec le Rayonnement Synchrotron (DESIRS) beam line at the Soleil Synchrotron facility [58] from the ground state and low-lying metastable states using light between 95 and 124 nm, reaching a precision of 750 MHz with spectral widths between 8.4 and 12 GHz.

There is limited work using the technique of saturated absorption spectroscopy on atomic nitrogen. These efforts focused on hyperfine structure and isotope shifts. In 1994, Cangiano *et al.* [59] reported measurements on the  $2p^2({}^3P)3s \ ^4P_{\frac{1}{2}-\frac{5}{2}} - 2p^2({}^3P)3p \ ^4P_{\frac{1}{2}-\frac{5}{2}}$  transitions. In 2006, Jennerich *et al.* [60] measured the same transitions and also the  $2p^2({}^3P)3s \ ^4P_{\frac{1}{2}-\frac{5}{2}} - 2p^2({}^3P)3p \ ^4P_{\frac{1}{2}-\frac{7}{2}}$  transitions. Jönsson *et al.* [61] calculated these hyperfine constants, identifying a large discrepancy with the experimentally reported hyperfine constants. This discrepancy was resolved by Carette *et al.* [62] who reanalyzed the spectrum, correctly identifying crossover features that complicated the original experimental analysis.

To our knowledge, the best reported value for the absolute transition frequencies concerning the transitions studied in this manuscript are from the original work by Eriksson in 1958 [47]. Eriksson used a nitrogen, neon, and helium mixture in a radio-frequency discharge. The Doppler broadened spectrum was measured using a spectrometer that had an accuracy of 0.002 nm (700 MHz).

A molecular transition overlaps the atomic transition  $({}^3P)3s \ ^2P_{3/2} - ({}^3P)3p \ ^2D_{5/2}^\circ$  near 939.5 nm. Our knowledge of these features was informed by Western *et al.* [63], who built upon the work of Boesch and Reiners [64] to compile nitrogen molecular lines between 637 and 2200 nm using the analysis program PGOPHER [65].

The paper is organized as follows: Section II describes the experimental setup. Section III presents results and a discussion of the systematic and statistical uncertainties that limit the precision of this experiment. Section IV concludes with a summary of the results.

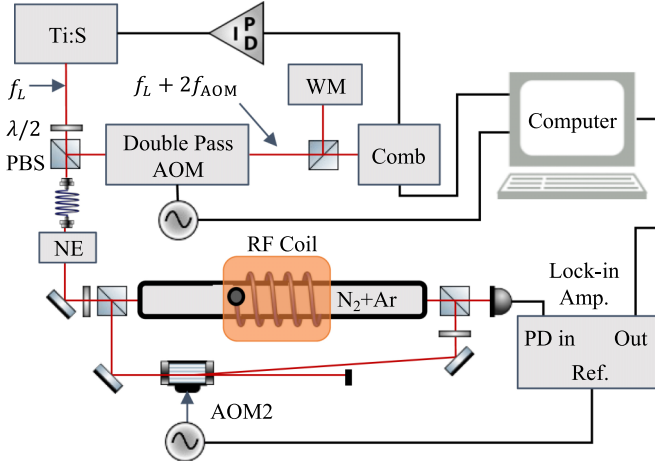


FIG. 2. Simplified experimental setup. Details are in the text. Ti:S: Titanium sapphire laser; AOM: acousto-optical modulator;  $\lambda/2$ : half-wave plate; PBS: polarizing beam splitter; WM: high-finesse wave meter; NE: noise eater; PD: photodiode.

## II. EXPERIMENTAL SETUP

A simplified experimental setup is shown in Fig. 2. A more thorough description of the experimental setup can be found in Ref. [66]. Briefly, a Ti-sapphire laser (MSquared SolsTiS) produces the laser light. The light is split by a polarizing beam-splitting cube, sending a portion to the saturated absorption setup and a portion to a double-pass acousto-optical modulator (AOM) (Brimrose GPM-800-200) setup [67]. The double-pass AOM has a center frequency of 800 MHz and a measured double-pass bandwidth of approximately 225 MHz. The frequency of the light after the double-pass AOM is given by  $f_L + 2f_{AOM}$ , where  $f_L$  is the frequency of the laser leaving the Ti:sapphire laser, and  $f_{AOM}$  is the frequency driving the AOM. The frequency-shifted light is then amplified before being sent to both a wave meter (High-Finesse/Angstrom WS7-30) and frequency comb (Toptica DFC).

The doubly diffracted light is beat against the frequency comb and stabilized using a proportional-integral-derivative (PID) controller (Toptica DigiLock) so that the laser is 20 MHz below a specified frequency comb mode. With the PID controller activated, the frequency of the light is fixed according to the equation

$$f_L = n f_{\text{rep}} + f_{\text{beat}} - 2f_{AOM}, \quad (1)$$

where  $n$  is the frequency comb order number,  $f_{\text{rep}} = 80$  MHz is the repetition rate of the frequency comb,  $f_{\text{beat}} = -20$  MHz is the beat frequency between the nearest frequency comb line and the laser beam, and  $2f_{AOM}$  is the frequency shift provided by the double-pass AOM setup. With the PID controller activated, changing  $f_{AOM}$  changes the frequency of the laser in a well-controlled, repeatable manner. This experimental setup allows the scanning of the laser frequency by over 600 MHz to a precision of better than 1.5 kHz. The data are collected by stepping the laser over the resonance region in 2 MHz steps. After the laser steps to a new frequency, a 60 ms pause (twice the 30 ms time constant of the lock-in amplifier) allows transient effects to settle before the signal intensity is collected and averaged over 100 ms.

The rest of the infrared light is fiber coupled to the saturated absorption setup. The waist of the laser leaving the fiber coupler is approximately 0.8 mm. The light is sent through a noise eater (Thorlabs NEL03A) to stabilize the intensity of the light. A half-wave plate and polarizing beam splitter are used to set the laser power of the probe beam. The pump beam passes through an AOM (ISOMET M1201-SF40-1.7) that is driven at 40 MHz and amplitude modulated. The diffracted pump beam's power is controlled by a second half-wave plate and polarizing beam splitter. The probe beam transmission is demodulated using the first harmonic by a lock-in amplifier (Stanford Research Systems SR830 DSP). Since the pump beam has a frequency that is 40 MHz larger than the probe beam, the resultant spectrum will be shifted 20 MHz lower than the actual zero Kelvin spectrum.

Molecular nitrogen and argon gas were mixed in a separate vacuum system before being leaked into a 500-mm-long borosilicate glass cell. Pressure ratios varying from 1.5% to 3% nitrogen by volume were used, as they produced the largest atomic signals. Other pressures were explored, including a pure nitrogen discharge, but a signal was not visible in the absence of argon. The atomic nitrogen was produced by a homemade rf coil with resonant frequency around 170 MHz. The frequency was supplied by a function generator (Stanford Research Systems SG384) amplified by a 20 Watt rf amplifier with a gain of 50 dB (Mini-Circuits ZHL-20W-13SW+).

## III. RESULTS AND DISCUSSION

The Hamiltonian that describes a particular hyperfine level is given by

$$H = A(\mathbf{I} \cdot \mathbf{J}) + B \frac{3(\mathbf{I} \cdot \mathbf{J})^2 + (3/2)(\mathbf{I} \cdot \mathbf{J}) - I(I+1)J(J+1)}{2I(2I-1)J(2J-1)}, \quad (2)$$

which leads to a hyperfine energy splitting from the center of gravity given by

$$\Delta E = \frac{1}{2}AK + B \frac{(3/2)K(K+1) - 2I(I+1)J(J+1)}{2I(2I-1)2J(2J-1)}, \quad (3)$$

where  $K = F(F+1) - I(I+1) - J(J+1)$ ,  $A$  is the magnetic dipole constant,  $B$  is the electric quadrupole constant,  $I$  is the nuclear spin,  $J$  is the total electronic angular momentum, and  $F$  is the total atomic angular momentum for a given hyperfine level. In this equation, the term with the electric quadrupole constant does not appear when  $J = 1/2$ .

The absolute transition frequency between any two hyperfine states is given by the equation

$$f = f_{\text{cog}} - aA_{LS} - bB_{LS} + a'A_{US} + b'B_{US}, \quad (4)$$

where  $A_{LS}$ ,  $B_{LS}$ ,  $A_{US}$ , and  $B_{US}$  are the magnetic dipole and electric quadrupole hyperfine constants of the lower and upper states, respectively.  $a$ ,  $b$ ,  $a'$ , and  $b'$  are determined from Eq. (3). In the absence of quantum interference [46], the relative amplitudes of the real transitions are given by

$$I_r = (2F+1)(2F'+1) \left\{ \begin{matrix} J & I & F \\ F' & 1 & J' \end{matrix} \right\}^2, \quad (5)$$

which are shown as insets in Fig. 1(a).

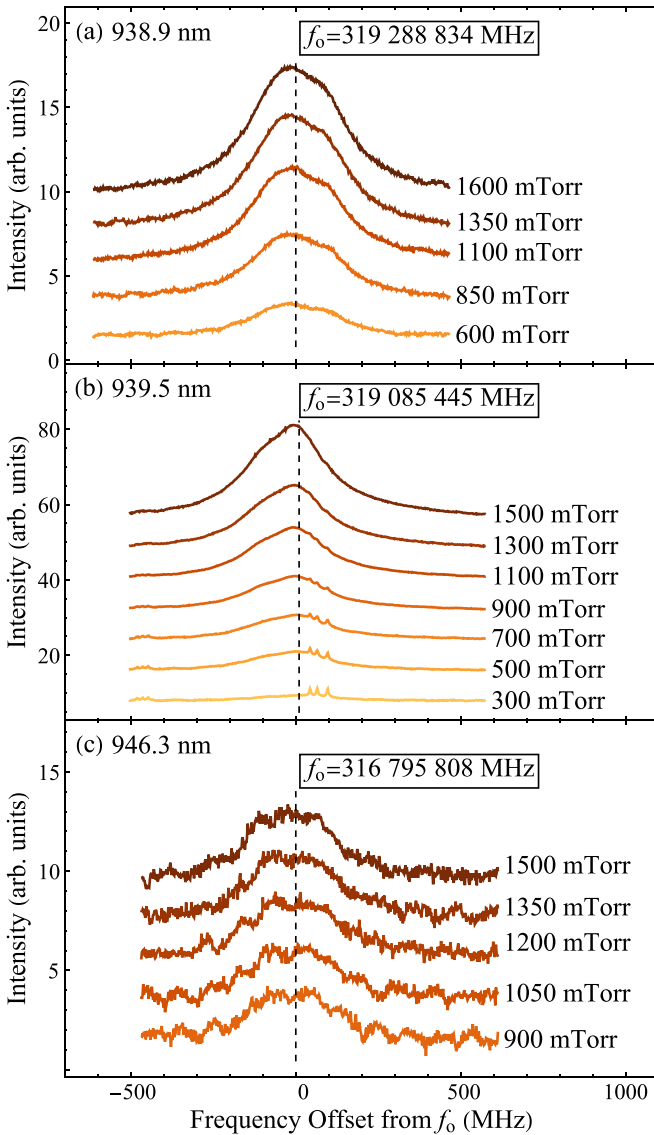


FIG. 3. Waterfall plots for varying discharge pressures for the three studied transitions. The transition near 939.5 nm has an overlapping nitrogen molecule line, which is more visible at smaller pressures. For presentation, each spectrum in a waterfall plot is the average of multiple spectra.

Spectra were obtained for the three transitions using a variety of experimental parameters including pressure, power driving the rf discharge, laser power, and laser alignment. These parameters can each, in principle, change the measured frequency of the transition. The total pressure was varied between 100 and 2000 mTorr. The power before the 20 W amplifier was varied between  $-10$  and  $0$  dBm. The total laser power was varied between  $1.0$  and  $5.6$  mW with a pump-probe power ratio of  $4.2$ . For each set of experimental parameters, at least four scans were collected. For lower pressure, low laser power, or low rf discharge power data, up to 10 scans were taken to average down the noise.

Figure 3 shows a waterfall plot for varying total pressures for all three studied transitions. The  $(^3P)3s^2P_{3/2} - (^3P)3p^2D_{5/2}^o$  transition near 939.5 nm has additional

spectral features, seen near  $-480$  and  $+80$  MHz on the horizontal axis. The work of Western *et al.* [63] indicates that these features are due to the molecular nitrogen line  $A^3\Sigma_u^+(\nu=4, J=13, N=12, F_1) - B^3\Pi_g(\nu=4, J=13, N=12, F_1)$ . The lower level of this molecular transition is metastable with a lifetime of about 2 seconds, so the widths of the spectral features are given by the transition natural linewidth broadened by laser power and discharge pressure. Each spectrum was fit to a sum of Lorentzian functions, whose centers are determined using Eq. (4), with equal full width half maxima plus a sloped offset using the *Mathematica* NonlinearModelFit function. The hyperfine constants, which were recently calculated by Jönsson and Godefroid [41], were taken to be known values, leaving the center of gravity transition frequency  $f_{\text{cog}}$  as the only fit parameter to determine the frequency offset of any spectral feature. NonlinearModelFit assumes that the original data points are independently normally distributed with a common standard deviation. The fit parameters are returned with uncertainty at the 95% confidence level.

Due to the merged spectrum, fitting is complicated by crossovers and possible quantum interference effects [46], which disallows a relationship between the real transition amplitudes given by Eq. (5). Including V crossovers and allowing the amplitudes of the Lorentzian functions to be free parameters, the resulting correlation matrix had large off-diagonal elements and large uncertainties on the center of gravity frequencies. However, the fitted value on  $f_{\text{cog}}$  could be reduced to sub-MHz precision if we incorrectly assumed the relative intensities of the real transitions are given by Eq. (5) and constrained the amplitudes of the V crossovers to reasonable values. We conclude that additional computational modeling of saturated absorption spectra with merged hyperfine structure is needed to find the relative amplitudes of the spectral features in order to extract  $f_{\text{cog}}$  to higher precision. With that modeling, a full systematic study of pressure shifts as well as possible shifts due to the rf discharge and laser power can be completed to obtain the center of gravity frequency to sub-MHz precision.

Due to this lack of knowledge in individual amplitudes, we make a conservative estimate of the center of gravity with uncertainty using the spectra with the lowest pressure; see Fig. 4. The lowest pressure data were also the noisiest data, so the scans were averaged together to increase the signal-to-noise ratio. After the scans were averaged, a small, laser-frequency-dependent oscillation with  $\approx 90$  MHz period was seen on all transitions. These oscillations are most clearly seen in Fig. 3(c). This oscillation was determined to be an atom-independent artifact of the experimental setup, likely a small etalon effect from the glass cell, and seen on the output of the lock-in amplifier in the absence of a discharge. Each spectrum was fit using the fit function described above plus a small amplitude sine wave to account for the atom-independent artifact. For the transition at 939.5 nm, six narrow Lorentzian features were added to the fit function to account for the molecular lines. Figure 4 shows the averaged data with the sloped offset and sinusoidal oscillation removed; for the 939.5 nm line, the molecular transitions were also removed for clarity of the center of gravity.

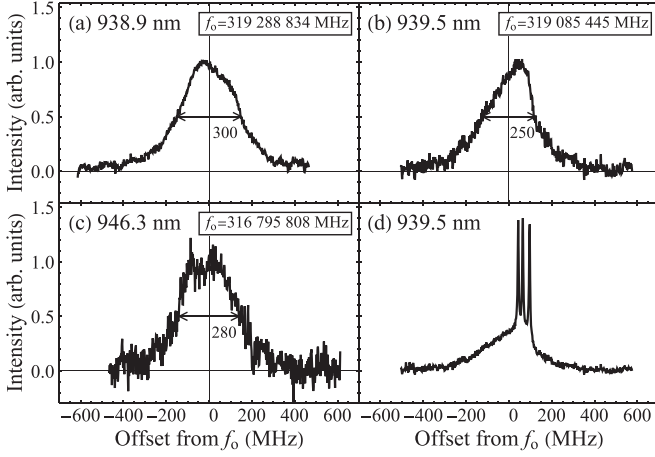


FIG. 4. Conservative estimates of the center of gravity with uncertainty. The large uncertainties are due to the merged hyperfine structure; see text for details. (a) The  $3s^2P_{1/2} - 3p^2D_{3/2}^{\circ}$  line near 938.9 nm using 600 mTorr of total pressure (1.5% nitrogen). (b) The  $3s^2P_{3/2} - 3p^2D_{5/2}^{\circ}$  line near 939.5 nm with the molecular line removed for visual purposes (see text for details) using 300 mTorr of total pressure (2.8% nitrogen). (c) The weaker  $3s^2P_{3/2} - 3p^2D_{3/2}^{\circ}$  line near 946.3 nm using 900 mTorr of total pressure (1.5% nitrogen). (d) The same as (b), but with the molecular lines included.

Our procedure for conservatively estimating the center of gravity with uncertainty is a three-step process. First, the fit function was used to find the frequency of the maximum value of the spectrum; the intensity of this maximum value is set to 1. Second, the same fit function was used to determine the frequencies at which the signal intensity is 0.5, or half of the maximum value. Finally, the center of gravity frequency is reported as the average of these two half-maxima frequency values. The uncertainty is half the difference of the half-maximum frequencies, as shown in Fig. 4. The summary of the results for this work is given in Table I. The uncertainties on the measurements are large enough that they encompass any shifts that might occur as a result of varying any of the systematics we tested, including the pressure shift.

If future QED calculations require higher-precision results, further theoretical support is needed to account for the hyperfine structure and to extract the center of gravity frequencies to higher precision. Constraining the relative amplitudes of the spectral features would likely allow fits with smaller off-diagonal elements for the correlation matrices and more certain results. The underlying data exploring systematics are available to allow others to explore fitting procedures.

If a better understanding of merged hyperfine structure cannot be developed on the theoretical front, it may be possible to produce resolved hyperfine spectra using crossover-free spec-

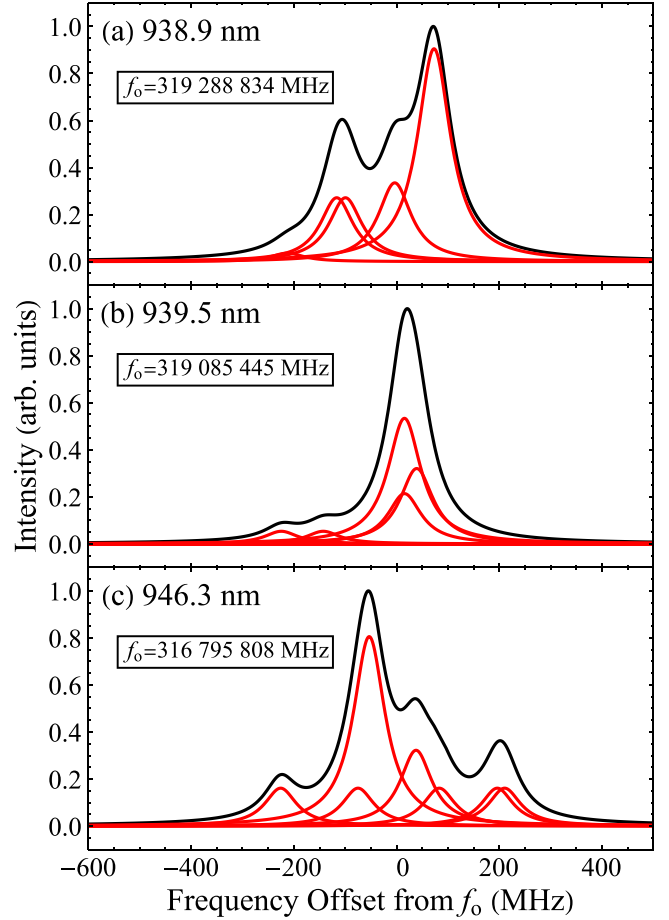


FIG. 5. Calculated spectrum for crossover free spectroscopy using the minimum possible FWHM for the spectral features with amplitudes calculated using Eq. (5). The red features are the contributions from each transition and the black feature is the predicted spectrum. Preliminary hyperfine constants were calculated by Jönsson and Godefroid [41,42]. To simulate these spectra, the constants used were  $A = 64.0$  MHz for the  $3s^2P_{1/2}$  state,  $A = 105.5$  MHz for the  $3s^2P_{3/2}$  state (at the time of this publication, the calculation of the hyperfine  $B$  constant for this state had not yet been finished),  $A = 70.6$  MHz and  $B = -3.176$  MHz for the  $3p^2D_{3/2}^{\circ}$  state, and  $A = 69.97$  MHz and  $B = -4.76$  MHz for the  $3p^2D_{5/2}^{\circ}$  state. (a) The  $3s^2P_{1/2} - 3p^2D_{3/2}^{\circ}$  line near 938.9 nm. (b) The  $3s^2P_{3/2} - 3p^2D_{5/2}^{\circ}$  line near 939.5 nm. (c) The weaker  $3s^2P_{3/2} - 3p^2D_{3/2}^{\circ}$  line near 946.3 nm.

troscopy [68] in a low-pressure environment. Figure 5 shows calculated crossover-free spectrums for all three transitions using preliminary hyperfine structure results from Jönsson and Godefroid [41,42] and assuming no quantum interference with the amplitudes of each transition given by Eq. (5). The

TABLE I. Absolute transition frequencies for all three studied transitions.

$\lambda$ (nm)	$f_{\text{cog}}$ (MHz)	Previous result [47] (MHz)	Transition
938.9	319 288 834(150)	319 289 000(700)	$3s^2P_{1/2} - 3p^2D_{3/2}^{\circ}$
939.5	319 085 445(125)	319 085 000(700)	$3s^2P_{3/2} - 3p^2D_{5/2}^{\circ}$
946.3	316 795 808(140)	316 796 000(700)	$3s^2P_{3/2} - 3p^2D_{3/2}^{\circ}$

FWHM of each spectral feature was found using  $\gamma = \gamma_{LS} + \gamma_{US}$ , where  $\gamma_{LS} = 1/\tau_{LS}$  is the linewidth of a  $3s^2P$  state and  $\gamma_{US} = 1/\tau_{US}$  is the linewidth of a  $3p^2D$  state. While slightly different for each transition, the FWHM are all  $\sim 80$  MHz. For clarity, the calculated spectrum for the 939.5 nm transition does not include the molecular lines.

#### IV. CONCLUSION

In this work, we present saturated absorption spectra of the three transitions connecting the  $2p^2(^3P)3s^2P_{1/2,3/2}$  and  $2p^2(^3P)3p^2D_{3/2,5/2}^o$  states in neutral  $^{14}\text{N}$ . A future two-photon experiment can be performed to improve upon the precision of the energy levels with respect to the ground state. The results in this manuscript are both a factor of five improvement in precision and in agreement with previous measurements. The precision is limited by an inability to predict the amplitude of the spectral features in the merged hyperfine structure. Extracting the center of gravity frequency to higher precision

will require additional theoretical support or new data collected using crossover-free spectroscopy. Improved modeling of merged hyperfine spectra will likely benefit the analysis of nine-electron systems, such as fluorine. Like nitrogen, all isotopes of fluorine, except  $^{16}\text{F}$  with a half life of  $21 \times 10^{-21}$  s, have nuclear spin, with most states having strong coupling to the ground state.

#### ACKNOWLEDGMENTS

This work was supported by the National Science Foundation through Grants No. PHY-1555232 and No. PHY-2110311. The authors would like to thank the Smith College Office of the Provost and Dean of Faculty for personnel support. The authors would also like to thank Maria-Teresa Herd of Assumption University, Timothy Malacarne of Nevada State University, and Patricia DiBartolo of Smith College for pedagogical discussions.

- 
- [1] K. T. Chung and X.-W. Zhu, Energies, fine structures, and isotope shifts of the  $1s^2snl$  excited states of the beryllium atom, *Phys. Rev. A* **48**, 1944 (1993).
  - [2] X.-W. Zhu and K. T. Chung, Energies, fine structures and oscillator strengths of  $1s^22p^2S$ ,  $^1D$  and  $^3P_{2,1,0}$  states of Be-like ions, *Phys. Scr.* **52**, 654 (1995).
  - [3] F. J. Gálvez, E. Buendía, and A. Sarsa, Excited states of beryllium atom from explicitly correlated wave functions, *J. Chem. Phys.* **117**, 6071 (2002).
  - [4] A. Aboussaid, M. R. Godefroid, P. Jönsson, and C. Froese Fischer, Multiconfigurational Hartree-Fock calculations of hyperfine-induced transitions in heliumlike ions, *Phys. Rev. A* **51**, 2031 (1995).
  - [5] A. M. Frolov and M. B. Ruiz, Bound state spectrum of the triplet states in the Be atom, *Chem. Phys. Lett.* **595-596**, 197 (2014).
  - [6] W. E. Caswell and G. P. Lepage, Effective Lagrangians for bound state problems in QED, QCD, and other field theories, *Phys. Lett. B* **167**, 437 (1986).
  - [7] J. S. Sims and S. Hagstrom, Combined configuration-interaction—hylleraas-type wave-function study of the ground state of the beryllium atom, *Phys. Rev. A* **4**, 908 (1971).
  - [8] A. Preiskorn and W. Woźnicki, Superposition of correlated configurations method. The ground state of  $H_3^+$ , *Chem. Phys. Lett.* **86**, 369 (1982).
  - [9] A. Preiskorn and W. Woźnicki, Variational calculations for the ground state of  $H_3^+$ , *Mol. Phys.* **52**, 1291 (1984).
  - [10] P. M. Kozłowski and L. Adamowicz, An effective method for generating nonadiabatic many-body wave function using explicitly correlated Gaussian-type functions, *J. Chem. Phys.* **95**, 6681 (1991).
  - [11] W. Cencek and J. Rychlewski, Many-electron explicitly correlated Gaussian functions. I. General theory and test results, *J. Chem. Phys.* **98**, 1252 (1993).
  - [12] S. A. Varganov and T. J. Martínez, Variational geminal-augmented multireference self-consistent field theory: Two-electron systems, *J. Chem. Phys.* **132**, 054103 (2010).
  - [13] G. W. F. Drake, M. M. Cassar, and R. A. Nistor, Ground-state energies for helium,  $\text{H}^-$ , and  $\text{Ps}^-$ , *Phys. Rev. A* **65**, 054501 (2002).
  - [14] P. J. Pelzl, G. J. Smethells, and F. W. King, Improvements on the application of convergence accelerators for the evaluation of some three-electron atomic integrals, *Phys. Rev. E* **65**, 036707 (2002).
  - [15] M. Puchalski and K. Pachucki, Ground-state wave function and energy of the lithium atom, *Phys. Rev. A* **73**, 022503 (2006).
  - [16] Z.-C. Yan, W. Nörtershäuser, and G. W. F. Drake, High precision atomic theory for Li and  $\text{Be}^+$ : QED shifts and isotope shifts, *Phys. Rev. Lett.* **100**, 243002 (2008).
  - [17] L. M. Wang, C. Li, Z.-C. Yan, and G. W. F. Drake, Isotope shifts and transition frequencies for the  $S$  and  $P$  states of lithium: Bethe logarithms and second-order relativistic recoil, *Phys. Rev. A* **95**, 032504 (2017).
  - [18] F. W. King, D. Quicker, and J. Langer, Compact wave functions for the beryllium isoelectronic series,  $\text{Li}^-$  to  $\text{Ne}^{6+}$ : A standard Hylleraas approach, *J. Chem. Phys.* **134**, 124114 (2011).
  - [19] K. Pachucki and J. Komasa, Relativistic and QED corrections for the beryllium atom, *Phys. Rev. Lett.* **92**, 213001 (2004).
  - [20] K. Pachucki and J. Komasa, Excitation energy of  $^9\text{Be}$ , *Phys. Rev. A* **73**, 052502 (2006).
  - [21] M. Stanke, D. Kedziera, S. Bubín, and L. Adamowicz, Lowest excitation energy of  $^9\text{Be}$ , *Phys. Rev. Lett.* **99**, 043001 (2007).
  - [22] S. Bubín, J. Komasa, M. Stanke, and L. Adamowicz, Isotope shifts of the  $1s^22s^2(^1S_0) \rightarrow 1s^22p^2(^1S_0)$  transition in the doubly ionized carbon ion  $\text{C}^{2+}$ , *Phys. Rev. A* **81**, 052504 (2010).
  - [23] S. Bubín, J. Komasa, M. Stanke, and L. Adamowicz, Isotope shifts of the three lowest  $^1S$  states of the  $\text{B}^+$  ion calculated with a finite-nuclear-mass approach and with relativistic and quantum electrodynamics corrections, *J. Chem. Phys.* **132**, 114109 (2010).
  - [24] M. Puchalski, K. Pachucki, and J. Komasa, Isotope shift in a beryllium atom, *Phys. Rev. A* **89**, 012506 (2014).

- [25] S. Bubin, M. Stanke, and L. Adamowicz, Non-Born–Oppenheimer calculations of the BH molecule, *J. Chem. Phys.* **131**, 044128 (2009).
- [26] M. Puchalski, J. Komasa, and K. Pachucki, Explicitly correlated wave function for a boron atom, *Phys. Rev. A* **92**, 062501 (2015).
- [27] G. W. Drake, Theoretical energies for the  $n = 1$  and 2 states of the helium isoelectronic sequence up to  $Z = 100$ , *Can. J. Phys.* **66**, 586 (1988).
- [28] V. M. Shabaev, Two-time Green’s function method in quantum electrodynamics of high- $Z$  few-electron atoms, *Phys. Rep.* **356**, 119 (2002).
- [29] V. A. Yerokhin, M. Puchalski, and K. Pachucki, QED calculation of the  $2p$  fine structure in Li-like ions, *Phys. Rev. A* **102**, 042816 (2020).
- [30] V. A. Yerokhin, V. Patkóš, and K. Pachucki, QED calculations of energy levels of heliumlike ions with  $5 \leq Z \leq 30$ , *Phys. Rev. A* **106**, 022815 (2022).
- [31] M. Puchalski, J. Komasa, and K. Pachucki, Testing quantum electrodynamics in the lowest singlet states of the beryllium atom, *Phys. Rev. A* **87**, 030502(R) (2013).
- [32] E. C. Cook, A. D. Vira, C. Patterson, E. Livernois, and W. D. Williams, Testing quantum electrodynamics in the lowest singlet state of neutral beryllium-9, *Phys. Rev. Lett.* **121**, 053001 (2018).
- [33] B. Maaß, T. Hütter, K. König, J. Krämer, J. Krause, A. Lovato, P. Müller, K. Pachucki, M. Puchalski, R. Roth, R. Sánchez, F. Sommer, R. B. Wiringa, and W. Nörtershäuser, Nuclear charge radii of  $^{10,11}\text{B}$ , *Phys. Rev. Lett.* **122**, 182501 (2019).
- [34] B. Maaß, Laser spectroscopy of the boron isotopic chain, Ph.D. thesis, Technische University Darmstadt, 2020, <http://dx.doi.org/10.25534/tuprints-00011484>.
- [35] A. Kramida, Yu. Ralchenko, J. Reader, and NIST ASD Team, NIST Atomic Spectra Database, ver. 5.10 (National Institute of Standards and Technology, Gaithersburg, MD, 2022), <https://physics.nist.gov/asd>.
- [36] K. Haris and A. Kramida, Critically evaluated spectral data for neutral carbon (C I), *Astrophys. J. Supplement Ser.* **233**, 16 (2017).
- [37] T. Otsuka, T. Suzuki, J. D. Holt, A. Schwenk, and Y. Akaishi, Three-body forces and the limit of oxygen isotopes, *Phys. Rev. Lett.* **105**, 032501 (2010).
- [38] E. Epelbaum, H.-W. Hammer, and Ulf-G. Meißner, Modern theory of nuclear forces, *Rev. Mod. Phys.* **81**, 1773 (2009).
- [39] J. Carlson, S. Gandolfi, F. Pederiva, S. C. Pieper, R. Schiavilla, K. E. Schmidt, and R. B. Wiringa, Quantum Monte Carlo methods for nuclear physics, *Rev. Mod. Phys.* **87**, 1067 (2015).
- [40] X. Yang, S. Wang, S. Wilkins, and R. G. Ruiz, Laser spectroscopy for the study of exotic nuclei, *Prog. Part. Nucl. Phys.* **129**, 104005 (2023).
- [41] P. Jönsson and M. Godefroid (private communication).
- [42] M. Ma, Y. Li, M. Godefroid, G. Gaigalas, J. Li, J. Bieroń, C. Chen, and P. Jönsson (unpublished).
- [43] G. Moon and H.-R. Noh, Analytic solutions for the saturated absorption spectra, *J. Opt. Soc. Am. B* **25**, 701 (2008).
- [44] G. Moon and H.-R. Noh, Analytic calculation of linear susceptibility in velocity-dependent pump-probe spectroscopy, *Phys. Rev. A* **78**, 032506 (2008).
- [45] H.-R. Noh, G. Moon, and W. Jhe, Discrimination of the effects of saturation and optical pumping in velocity-dependent pump-probe spectroscopy of rubidium: A simple analytical study, *Phys. Rev. A* **82**, 062517 (2010).
- [46] R. C. Brown, S. Wu, J. V. Porto, C. J. Sansonetti, C. E. Simien, S. M. Brewer, J. N. Tan, and J. D. Gillaspay, Quantum interference and light polarization effects in unresolvable atomic lines: Application to a precise measurement of the  $^{6,7}\text{Li } D_2$  lines, *Phys. Rev. A* **87**, 032504 (2013).
- [47] K. B. S. Eriksson, Revised energy levels for the neutral nitrogen atom, *Ark. Fys.* **13**, 429 (1958).
- [48] K. B. S. Eriksson and I. Johansson, The spectrum of the neutral nitrogen atom in the lead-sulfide region, *Ark. Fys.* **19**, 235 (1961).
- [49] V. Kaufman and J. F. Ward, Newly measured and calculated wavelengths in the vacuum ultraviolet spectrum of neutral nitrogen, *Appl. Opt.* **6**, 43 (1967).
- [50] K. B. S. Eriksson and J. E. Pettersson, New measurements in the spectrum of the neutral nitrogen atom, *Phys. Scr.* **3**, 211 (1971).
- [51] K. B. S. Eriksson, An Extension of the Analysis of N I, *Phys. Scr.* **9**, 151 (1974).
- [52] K.-B. S. Eriksson, Additions to the Spectrum of the Neutral Nitrogen Atom, *Phys. Scr.* **34**, 211 (1986).
- [53] C. E. Moore, *Selected tables of atomic spectra – A: atomic energy levels (2nd ed.) – B: multiplet table: N I, N II, N III. Data derived from the analyses of optical spectra*, Nat. Stand. Ref. Data Ser., Nat. Bur. Stand. Report NSRDS-NBS3, Washington DC (1975), <https://www.nist.gov/srd/national-standard-reference-data-series>.
- [54] C. E. Moore, *Tables of Spectra of Hydrogen, Carbon, Nitrogen, and Oxygen*, edited by J. W. Gallagher (CRC Press, Inc., Boca Raton, FL, 1993).
- [55] S. Hannemann, U. Hollenstein, E.-J. van Duijn, and W. Ubachs, Production of narrowband tunable extreme-ultraviolet radiation by noncollinear resonance-enhanced four-wave mixing, *Opt. Lett.* **30**, 1494 (2005).
- [56] E. J. Salumbides, J. P. Sprengers, E. Reinhold, and W. Ubachs, High precision frequency calibration of N I lines in the XUV domain, *J. Phys. B: At., Mol. Opt. Phys.* **38**, L383 (2005).
- [57] K.-F. Lai, W. Ubachs, N. De Oliveira, and E. J. Salumbides, Fourier-Transform VUV Spectroscopy of  $^{14,15}\text{N}$  and  $^{12,13}\text{C}$ , *Atoms* **8**, 62 (2020).
- [58] N. de Oliveira, D. Joyeux, M. Roudjane, J.-F. Gil, B. Pilette, L. Archer, K. Ito, and L. Nahon, The high-resolution absorption spectroscopy branch on the VUV beamline DESIRS at SOLEIL, *J. Synchrotron Radiat.* **23**, 887 (2016).
- [59] P. Cangiano, M. de Angelis, L. Gianfrani, G. Pesce, and A. Sasso, Hyperfine-Structure and Isotope-Shift Investigations of Atomic Nitrogen by Saturation Spectroscopy, *Phys. Rev. A* **50**, 1082 (1994).
- [60] R. M. Jennerich, A. N. Keiser, and D. A. Tate, Hyperfine structure and isotope shifts in near-infrared transitions of atomic nitrogen, *Euro. Phys. J. D* **40**, 81 (2006).
- [61] P. Jönsson, T. Carette, M. Nemouchi, and M. Godefroid, *Ab initio* calculations of  $^{14}\text{N}$  and  $^{15}\text{N}$  hyperfine structures, *J. Phys. B: At. Mol. Opt. Phys.* **43**, 115006 (2010).
- [62] T. Carette, M. Nemouchi, P. Jönsson, and M. Godefroid, Saturation spectra of low lying states of nitrogen: Rec-

- onciling experiment with theory, *Europhys. J. D* **60**, 231 (2010).
- [63] C. M. Western, L. Carter-Blatchford, P. Crozet, A. J. Ross, J. Morville, and D. W. Tokaryk, The spectrum of N<sub>2</sub> from 4,500 to 15,700 cm<sup>-1</sup> revisited with PGOPHER, *J. Quantum Spectrosc. Radiat. Transfer* **219**, 127 (2018).
- [64] A. Boesch and A. Reiners, Spectral line lists of a nitrogen gas discharge for wavelength calibration in the range 4500–11,000 cm<sup>-1</sup>, *A&A* **582**, A43 (2015).
- [65] C. M. Western, PGOPHER: A program for simulating rotational, vibrational and electronic spectra, *J. Quantum Spectrosc. Radiat. Transfer* **186**, 221 (2017).
- [66] M. T. Herd, C. Maruko, M. M. Herzog, A. Brand, G. Cannon, B. Duah, N. Hollin, T. Karani, A. Wallace, M. Whitmore, and W. D. Williams, Spectroscopic study of the  $4f^7 6s^2 8S_{7/2}^{\circ} - 4f^7 ({}^8S^{\circ}) 6s 6p ({}^1P^{\circ}) 8P_{9/2}$  transition in neutral europium-151 and europium-153: Absolute frequency and hyperfine structure, *J. Opt. Soc. Am. B* **39**, 2596 (2022).
- [67] E. A. Donley, T. P. Heavner, F. Levi, M. O. Tataw, and S. R. Jefferts, Double-pass acousto-optic modulator system, *Rev. Sci. Instrum.* **76**, 063112 (2005).
- [68] A. Banerjee and V. Natarajan, Saturated-absorption spectroscopy: Eliminating crossover resonances by use of copropagating beams, *Opt. Lett.* **28**, 1912 (2003).